Review of Scientific Instruments

RESEARCH ARTICLE | JULY 17 2013

Novel *in situ* cell for Raman diagnostics of lithium-ion batteries

T. Gross; L. Giebeler; C. Hess

Rev. Sci. Instrum. 84, 073109 (2013)
https://doi.org/10.1063/1.4813263

AIP Publishing

Novel *in situ* cell for Raman diagnostics of lithium-ion batteries

T. Gross, L. Giebeler,[a] and C. Hess[b]
Eduard-Zintl-Institut für Anorganische und Physikalische Chemie, Technische Universität Darmstadt, Petersenstr. 20, 64287 Darmstadt, Germany

(Received 15 February 2013; accepted 22 June 2013; published online 17 July 2013)

A novel *in situ* cell for Raman diagnostics of working lithium-ion batteries is described. The design closely mimics that of standard battery testing cells and therefore allows to obtain Raman spectra under representative electrochemical conditions. Both cathode and anode materials can be studied. First results on the intercalation of a $Li_{1-x}CoO_2$ cathode material demonstrate the potential of the experimental approach for structural studies and underline the importance of studying lithium-ion batteries at work. © *2013 AIP Publishing LLC*. [http://dx.doi.org/10.1063/1.4813263]

I. INTRODUCTION

Secondary lithium-ion batteries are based on the intercalation of lithium into a variety of host materials. The loss of electrochemical performance as a result of successive charge-discharge cycles is still a major problem of such systems hampering their application, e.g., as power source in electric vehicles. Among other aspects, rational development of improved secondary lithium-ion batteries will require a thorough understanding of the structural properties of electrode materials under working conditions of the battery. Raman spectroscopy is a non-destructive optical method that probes the local structure of solids under a multitude of reaction environments. It has been shown that Raman spectroscopy is a powerful tool to study secondary lithium-ion battery electrodes providing valuable information, e.g., on the nature and crystallinity of electrode phases (phase identification), local disorder, variations in bond lengths and coordination. To this end, carbonaceous negative electrodes and (lithiated) transition metal-oxide based positive electrodes have been extensively studied in the past.[1] More recent studies have demonstrated the potential of Raman spectroscopy for *in situ* characterization of electrode materials of lithium-ion batteries even at the single particle level.[2–6,8,9,15,16,20,21,26]

The ultimate goal of *in situ* battery characterization is to monitor electrode materials at work (*operando* spectroscopy) to unravel the material properties responsible for electrochemical performance. In the following, we present a novel *in situ* Raman cell design, which allows to record spectra under representative electrochemical conditions and which unlike previous cell designs closely mimics that of standard battery testing cells.[15,17,20,22]

It is known from the literature that the Raman spectrum of hexagonal $LiCoO_2$ is characterized by two Raman bands at around 485 and 595 cm^{-1}, respectively, corresponding to oxygen vibrations involving mainly O–Co–O bending (E_g) and Co–O stretching (A_{1g}).[6,7,10] Regarding $LiCoO_2$-based positive electrodes *in situ* Raman spectroscopy has been employed to study commercial powder $LiCoO_2$ electrodes[21] and the deintercalation of thin film electrodes of pure $LiCoO_2$.[9] The reported thin film Raman data are in contrast with work by Inaba *et al.*[6] regarding spectral behavior during lithium deintercalation of $LiCoO_2$, which has been explained by the specific structural response of a $LiCoO_2$ thin film differing from that of $LiCoO_2$ powder.[13] To further elucidate the factors determining the spectral changes of $LiCoO_2$ based electrodes, we present new results on the *in situ* intercalation of a $LiCoO_2$ powder containing binder and carbon additives (cathode mix).

II. EXPERIMENTAL SETUP FOR RAMAN DIAGNOSTICS

$LiCoO_2$ was prepared by a modified *Pechini* process using appropriated amounts of lithium nitrate and cobalt nitrate(-hydrate) as initial reagents. Both were dissolved in water and a double amount (w/w) of citric acid as complexing agent. Ammonia solution was added until the pH value of the solution was equal to 5. A fourfold amount (with respect to the mass of citric acid) of ethylene glycol was added. The solution was heated stepwise up to 180 °C resulting in formation of a dried precipitate. The product was ground and pre-calcined at 450 °C in air for 6 h, then ground again and finally calcined at 800 °C in air for 20 h. The composite electrode was done by thoroughly mixing 84% of active material ($LiCoO_2$), 8% carbon black, and 8% polyvinylidene difluoride (PVDF) in a mortar. Approximately 10 mg of cathode mixture was pressed onto an aluminium grid with 3 t for 30 s in a hydraulic press.

Figure 1 shows a scheme of the complete experimental setup for Raman diagnostics of powder electrodes. In the following, we discuss details of the Raman spectrometer. The design of the *in situ* Raman cell will be described in Sec. II B. In Sec. II C, the design and assembly of the Raman cell will be illustrated by photographs.

A. Raman spectrometer

For Raman experiments, 514.5 nm excitation from an Ar-ion laser (Melles Griot) was employed. The laser was operated at a power level of 7 mW as measured at the position of the sample using a power meter (Ophir). The laser beam

[a]Present address: Leibniz-Institut für Festkörper- und Werkstoffforschung Dresden e.V., Helmholtzstraße 20, 01069 Dresden, Germany.
[b]Author to whom correspondence should be addressed. Electronic mail: hess@pc.chemie.tu-darmstadt.de

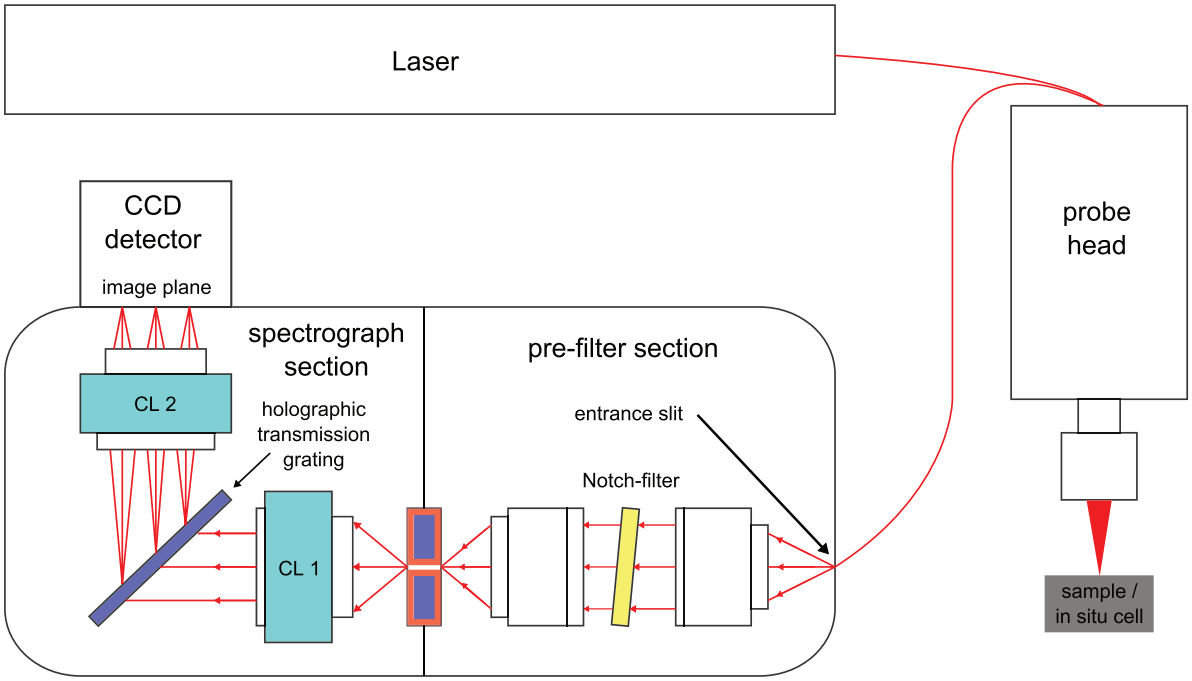

FIG. 1. Experimental setup for Raman diagnostics. For details, see text.

is guided to the sample by a one-in/one-out quartz fibre optic connected to a MKII-filtered probe head (Kaiser Optical, see Fig. 1) mounted on a x-y-z stage (Newport); it is then focussed onto the sample (located in the mounted cell) using a high precision microscope objective (Olympus SLMPLN 20×0.25). The spot size of the laser beam at the sample position is approximately 2–3 μm in diameter as calculated with parameters from the data sheet of the objective. Raman light is scattered from the sample in a 180°-backscattering geometry and sent to a transmission spectrometer (Kaiser Optical, HL5R) equipped with an electrically cooled CCD detector (Andor, see Fig. 1) with 256 × 1024 pixels. The spectrometer was calibrated using the emission lines of an Ar lamp. To block the elastically scattered light, two SuperNotch Plus filters (Kaiser Optical) were employed. The resolution of this instrument is 5 cm^{-1}; however, the wavelength reproducibility is better than 0.5 cm^{-1}.

B. Design of the *in situ* cell

Figure 2 gives a cross-sectional view of the novel *in situ* Raman cell. The cell chassis consists of a Swagelok perfluoroalkoxy (PFA) straight screwed coupling with 0.5 in. inner diameter (see Fig. 2, light grey center part). One of the original screw nuts is kept as cell bottom to hold the cathode stainless steel current collector. So effectively, one half of the *in situ* cell is equivalent to the standard Swagelok battery testing cell. The upper current collector (in darkish grey on the right side of Fig. 2) is connected to the optical window insertion device which presses on to the assembled electrodes from one side. The other current collector exhibits a small force onto the assembly via a steel spring (which is also the electrical contact) pressing on a nickel plate and accounts for changes in volume that might occur during electrochemical cycling. The battery cell consists of two electrodes separated by several layers of glass fibre filter paper soaked with electrolyte to prevent a short circuit.

The design of the cell allows for two measurement modes:

(A) The electrode is measured as bottom electrode (see Fig. 2). For this purpose, a hole (diameter: 1–5 mm) needs to be blanked into the lithium metal (anode or negative electrode) and the separators to allow the laser beam to pass. The drawback of this setup is that the area which is usually examined (the center of the electrode) may not have the optimum contact to its counter-electrode via the separators. This potential problem can be overcome when measuring at the outer rim of the electrode.

(B) The electrode is measured as top electrode. The reverse assembly of the cathode-separators-anode part is also

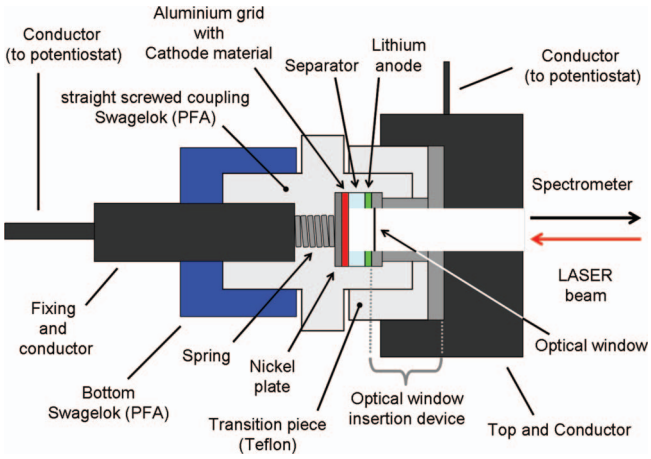

FIG. 2. Cross-section of the *in situ* Raman cell for diagnostics of lithium-ion batteries.

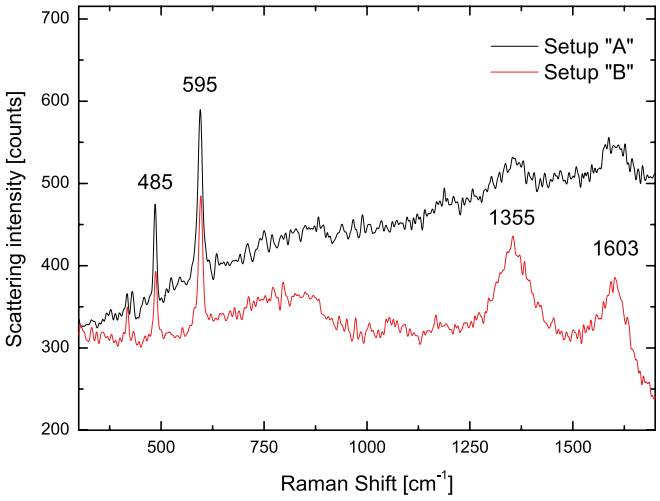

FIG. 3. *In situ* Raman spectra of a $LiCoO_2$ composite cathode recorded in measurement modes (A) and (B) using the same experimental conditions.

possible. The cathode mixture is usually pressed on a aluminum grid. The mesh size of the grid is about an order of magnitude smaller than the laser beam diameter. Therefore, it is quite suitable to guide the laser beam through any given mesh of the aluminum grid. The good electrochemical contact of the "backside" of the electrode is evidenced by the detection of Raman bands of the electrolyte solvents (see discussion below).

Either mode allows for measurements on positive electrodes and negative electrodes. Charges are collected with crocodile clamps from stainless steel screws connected to the current collectors. The tightness against moisture and air is provided by the original Swagelok gasket rings for the bottom part of the cell. Such a gasket system keeps the tubings gas-tight enabling them even for hydrogen use. To seal off the upper part of the *in situ* cell, Viton-O ring seals are mounted into the window insertion device and between the transition piece and the upper current collector. The optical window insertion device is made of two parts: the upper part fixes the sapphire window (or alternatively the optical quartz window), the lower part serves as window socket. Both parts are connected through a screw thread. As the insertion device is made of stainless steel, it also serves as electrical connection to the current collector. For the two measurement modes, similar Raman spectra of $LiCoO_2$-based composite electrodes were obtained (see Fig. 3). The overall thickness of the measured cathode is approximately 0.2 mm. For comparison, due to the presence of strongly absorbing carbon the penetration depth of the photons is estimated to be a few hundred nanometers, as confirmed by Raman experiments on amorphous carbon materials conducted at 514.5 nm excitation.[25] All measurements shown here were acquired in measurement mode (B).

C. Assembly of the *in situ* cell

Figure 4 summarizes different stages of the assemblage of the *in situ* cell. The fully mounted cell is shown at various angles in parts (a) and (d), respectively. Picture (d) displays the stainless steel top housing the optical window (sapphire).

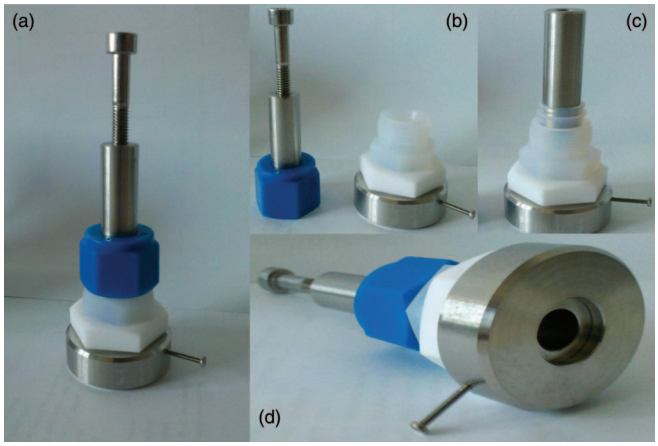

FIG. 4. (a)–(d) Photographs of the assemblage of the *in situ* Raman cell.

Pictures (b) and (c) illustrate different stages of assembly: (b) blue PFA straight screwed coupling with stainless steel current collector and the upper white-transparent part of the screw coupling, (c) standard Swagelok gasket rings assuring gas-tightness connecting the stainless steel current collector with the other parts of the cell.

III. ELECTROCHEMICAL PERFORMANCE

The electrochemical performance of the novel *in situ* cell was tested using cyclic voltammetry and galvanostatic cycling (potentiostat VSP, BioLogic). As positive electrode, a cathode mix (84% active material, 8% carbon, 8% PVDF) with $LiCoO_2$ as active material was used; Li metal served as counter electrode. A commercially available standard electrolyte was employed (1 M $LiPF_6$ in ethylene carbonate (EC):dimethyl carbonate (DMC) 1:1 (wt.); LP 30, Merck).

Figure 5(A) shows the results of a standard program for cyclic voltammetry (scanning rate of 0.05 mV/s) of the first four electrochemical cycles. The peaks at 3.98, 4.09, and 4.19 V (in positive scanning direction) as well as those in reverse direction at 3.87, 4.05, and 4.15 V are in good agreement with those reported in literature for $LiCoO_2$[23,24] and indicate good reversibility of the electrochemical reaction. Figure 5(B) demonstrates the reproducibility of the *in situ* Raman cell. The spectra shown were taken in subsequent cycles in the course of an *in situ* experiment at the same degree of intercalation ($x = 0.5$). Note that the spectra have been offset for clarity, but are otherwise untreated raw data (no background subtraction, normalization). The grey areas mark the positions of the A_{1g} and E_g modes of the active material. Besides the peak at 417 cm^{-1}, all other features can be assigned to the aprotic solvents ethylene carbonate and dimethyl carbonate (see discussion below). The peak at 417 cm^{-1} is due to the optical window material (sapphire). It should be mentioned that there is nothing peculiar about the fact that the 485 cm^{-1} peak is not "visible" in some spectra (e.g., spectrum #3_{ins}) considering the relative ratio of the 485 cm^{-1} and 595 cm^{-1} peak intensities as well as the noise level in the series of spectra.

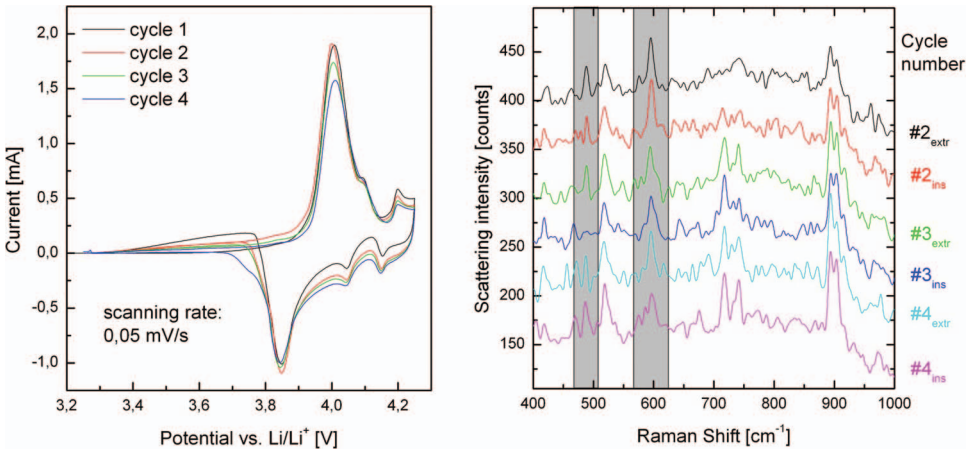

FIG. 5. *In situ* Raman spectroscopy during electrochemical cycling. (a) Cyclic voltammograms of the first four cycles. (b) Corresponding *in situ* Raman spectra recorded at the same degree of intercalation ($x = 0.5$). Grey markers display the position of phonon bands of the active material. Subscripts "extr" and "ins" indicate Li extraction and insertion, respectively. For details, see text.

IV. RAMAN DIAGNOSTICS DURING INTERCALATION

The potential of the novel *in situ* cell is highlighted by studies on the deintercalation of a cathode mix with $LiCoO_2$ as active material. The cathode mix was composed of 84% $LiCoO_2$, 8% PVDF, and 8% Carbon black; the electrolyte consisted of 1 M $LiPF_6$ dissolved in a 1:1 mixture (wt.) of ethylene carbonate/dimethyl carbonate. Galvanostatic cycling was performed at a cycling rate of C/15 (corresponding to $\sim$19.0 mAg^{-1}) by using potential limits of $E_{min} = 2.7$ V and $E_{max} = 4.2$ V. Raman spectra were continuously acquired every 36 min in the "backside" geometry.[18]

Figures 6 and 7 give different representations of a series of *in situ* Raman spectra during electrochemical $Li_{1-x}CoO_2$ de-intercalation and intercalation taken during the third cycle. In Figure 6, spectra are offset to clearly display the spectral evolution during galvanostatic cycling. The spectra are characterized by two Raman bands at 485 and 595 cm^{-1} (marked grey areas), which are attributed to O–Co–O bending (E_g) and Co–O stretching (A_{1g}), respectively, in accordance with the literature.[6,7,10] Assignment of the electrolyte-related Raman features is as follows: the peak at 742 cm^{-1} originates from the totally symmetric vibration of the PF_6^- anion, peaks at 716 and 894 cm^{-1} are due to the C=O-ring bending (out of plane) and the ring breathing mode of the ethylene carbonate solvent and peaks at 519 and 918 cm^{-1} are attributed to the O–C–O bending and the CH_3–O stretching modes of dimethyl carbonate.[11,14] The feature at 904 cm^{-1} results from the

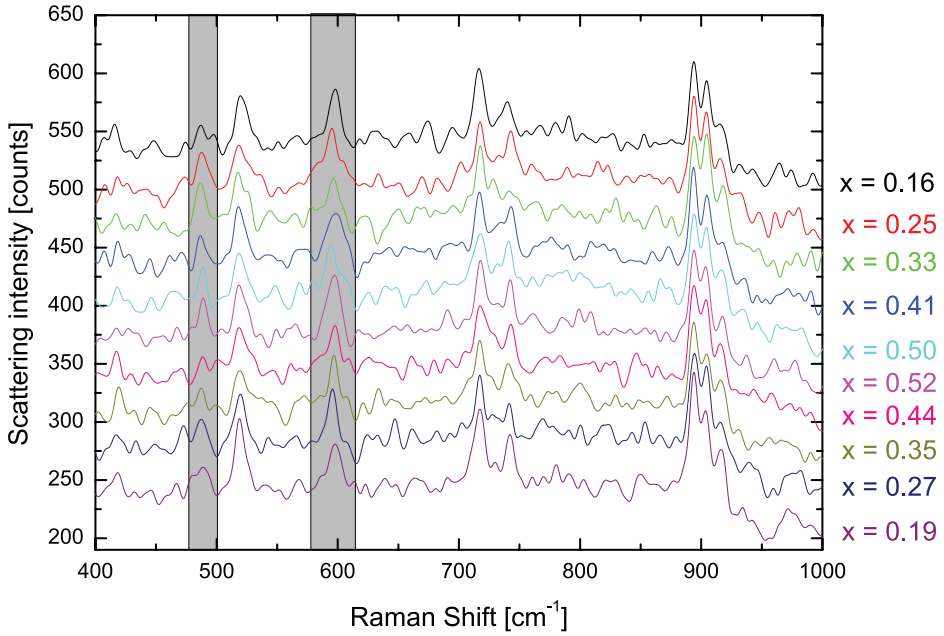

FIG. 6. *In situ* Raman spectra of a $Li_{1-x}CoO_2$ cathode mix upon galvanostatic cycling. The spectra were offset for clarity. Grey markers display the position of the active material phonon bands. For details, see text.

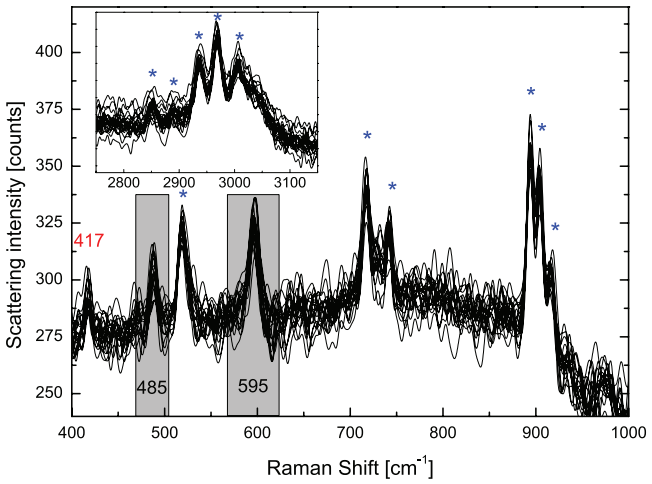

FIG. 7. *In situ* Raman raw data of a $Li_{1-x}CoO_2$ cathode mix upon galvanostatic cycling recorded during one complete cycle (19 spectra). The inset shows the corresponding spectra of the high-frequency region. Asterisks mark the positions of the solvent signals. For details, see text.

interaction of $LiPF_6$ with both solvents, whereas the peaks in the high-frequency range 2850–3050 cm^{-1} result from C–H stretching modes of EC/DMC.[11,14] The fact that electrolyte signals are observed, strongly indicates that the electrode is fully immersed in the electrolyte during experiments.

To demonstrate the stability of the setup, Fig. 7 shows the same series of spectra as raw data, i.e., without subtraction of background, normalization, or offset. In particular, the uniformity of the spectral quality is underlined, i.e., the sample remains focussed during measurement, the background level stays constant, and the electrode environment remains the same during the whole cycle. The positions of the $Li_{1-x}CoO_2$ phonon bands are marked grey areas, the sapphire peak in red. Blue asterisks indicate the positions of signals that are attributed to the electrolyte. The inset displays the corresponding high-frequency region of the spectra, showing more aprotic solvents signals. The figure also demonstrates that the position of the E_g and A_{1g} phonon bands is almost indifferent

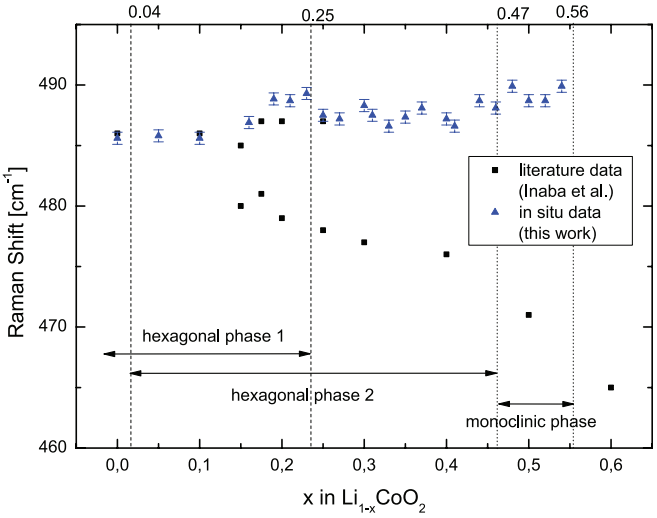

FIG. 8. Comparison of *in situ* Raman data from this work with *ex situ* data from the literature.[6]

to changes via electrochemical cycling, as discussed in more detail in the following.

Figure 8 compares *in situ* Raman data from this work with Raman data on $LiCoO_2$ powder reported in the literature.[6] The literature data is termed *ex situ* as spectra were recorded after electrochemical lithium deintercalation and subsequent removal of the electrode material from the electrochemical environment.

In Fig. 8, the frequency position of the 485 cm^{-1} E_g phonon is displayed as a function of Li content.[19] There is a striking difference between the spectral behavior observed under *in situ* and *ex situ* conditions. Under *in situ* conditions the frequency of the E_g band varies insignificantly during lithium deintercalation while *ex situ* spectra show a redshift of more than 20 cm^{-1}. The spectral changes have been correlated with structural changes associated with phase transitions in $LiCoO_2$, i.e., transitions between two hexagonal phases and between a hexagonal and a monoclinic phase, respectively, as confirmed by X-ray diffraction.[6] In contrast, the spectral invariance observed under *in situ* conditions does not indicate any structural changes of $LiCoO_2$ during deintercalation. Considering the discussion on the origin of fatigue of $LiCoO_2$-based materials,[12] the observed behavior underlines the importance of studying lithium-ion batteries at work.

V. SUMMARY

A novel *in situ* Raman cell has been designed, built, and successfully tested for lithium-ion batteries by monitoring Raman spectra during deintercalation of a $Li_{1-x}CoO_2$ cathode material. The difference to deintercalation data obtained by *ex situ* characterization underlines the importance of *in situ* Raman diagnostics for understanding the fatigue of lithium-ion batteries.

ACKNOWLEDGMENTS

The financial support of this work by the *Deutsche Forschungsgemeinschaft* (DFG) in the frame of project B8 within *Sonderforschungsbereich 595* "Electrical fatigue in functional materials" is gratefully acknowledged. We are indebted to Dipl.-Ing. Robert Gunkel and Dipl.-Ing. Karl Kopp for helpful discussions and assistance in construction as well as the workshop of the Department of Chemistry for manufacture. The authors wish to thank Julia Eigenseer and Marcel Heber for their help with some of the Raman measurements.

[1]R. Baddour-Hadjean and J.-P. Pereira-Ramos, "Raman microspectrometry applied to the study of electrode materials for lithium batteries," Chem. Rev. **110**(3), 1278–1319 (2010).
[2]K. Dokko, N. Anzue, M. Mohamedi, T. Itoh, and I. Uchida, "Raman spectro-electrochemistry of $LiCo_xMn_{2-x}O_4$ thin film electrodes for 5 V lithium batteries," Electrochem. Commun. **6**(4), 384–388 (2004).
[3]K. Dokko, M. Mohamedi, N. Anzue, T. Itoh, and I. Uchida, "*In situ* Raman spectroscopic studies of $LiNi_xMn_{2-x}O_4$ thin film cathode materials for lithium ion secondary batteries," J. Mater. Chem. **12**(12), 3688–3693 (2002).
[4]K. Dokko, Q. Shi, I. C. Stefan, and D. A. Scherson, "*In situ* Raman spectroscopy of single microparticle Li^+-intercalation electrodes," J. Phys. Chem. B **107**(46), 12549–12554 (2003).
[5]W. Huang and R. Frech, "*In situ* Raman spectroscopic studies of electrochemical intercalation in $Li_xMn_2O_4$-based cathodes," J. Power Sources **81–82**, 616–620 (1999).

[6]M. Inaba, Y. Iriyama, Z. Ogumi, Y. Todzuka, and A. Tasaka, "Raman study of layered rock-salt $LiCoO_2$ and its electrochemical lithium deintercalation," J. Raman Spectrosc. **28**(8), 613–617 (1997).
[7]M. Inaba, Y. Todzuka, H. Yoshida, Y. Grincourt, A. Tasaka, Y. Tomida, and Z. Ogumi, "Raman spectra of $LiCo_{1-y}Ni_yO_2$," Chem. Lett. **24**(10), 889–890 (1995).
[8]T. Itoh, N. Anzue, M. Mohamedi, Y. Hisamitsu, M. Umeda, and I. Uchida, "Spectroelectrochemical studies on highly polarized $LiCoO_2$ electrode in organic solutions," Electrochem. Commun. **2**(11), 743–748 (2000).
[9]T. Itoh, H. Sato, T. Nishina, T. Matue, and I. Uchida, "*In situ* Raman spectroscopic study of Li_xCoO_2 electrodes in propylene carbonate solvent systems," J. Power Sources **68**(2), 333–337 (1997).
[10]C. Julien, "Local cationic environment in lithium nickel–cobalt oxides used as cathode materials for lithium batteries," Solid State Ionics **136–137**, 887–896 (2000).
[11]J. E. Katon and M. D. Cohen, "The vibrational spectra and structure of dimethyl carbonate and its conformational behavior," Can. J. Chem. **53**(9), 1378–1386 (1975).
[12]M. Kerlau, M. Marcinek, V. Srinivasan, and R. M. Kostecki, "Studies of local degradation phenomena in composite cathodes for lithium-ion batteries," Electrochim. Acta **52**(17), 5422–5429 (2007).
[13]Y. J. Kim, E.-K. Lee, H. Kim, J. Cho, Y. W. Cho, B. Park, S. Mo Oh, and J. K. Yoon, "Changes in the lattice constants of thin-film $LiCoO_2$ cathodes at the 4.2 V charged state," J. Electrochem. Soc. **151**(7), A1063–A1067 (2004).
[14]B. Klassen, R. Aroca, M. Nazri, and G. A. Nazri, "Raman spectra and transport properties of lithium perchlorate in ethylene carbonate based binary solvent systems for lithium batteries," J. Phys. Chem. B **102**(24), 4795–4801 (1998).
[15]J. Lei, F. McLarnon, and R. Kostecki, "*In situ* Raman microscopy of individual $LiNi_{0.8}Co_{0.15}Al_{0.05}O_2$ particles in a Li-ion battery composite cathode," J. Phys. Chem. B **109**(2), 952–957 (2005).
[16]Y. Luo, W.-B. Cai, X.-K. Xing, and D. A. Scherson, "*In situ*, time-resolved Raman spectromicrotopography of an operating lithium-ion battery," Electrochem. Solid-State Lett. **7**(1), E1–E5 (2004).
[17]S. Migge, G. Sandmann, D. Rahner, H. Dietz, and W. Plieth, "Studying lithium intercalation into graphite particles via *in situ* Raman spectroscopy and confocal microscopy," J. Solid State Electrochem. **9**(3), 132–137 (2005).
[18]The acquisition time of 36 min corresponds to $\Delta x \approx 0.05$ (5% Li). Please note that Figure 6 does not show all 19 spectra that were recorded during one full cycle.
[19]A similar behavior is observed for the 595 cm^{-1} A_{1g} phonon feature (not shown).
[20]P. Novák, D. Goers, L. Hardwick, M. Holzapfel, W. Scheifele, J. Ufheil, and A. Würsig, "Advanced *in situ* characterization methods applied to carbonaceous materials," J. Power Sources **146**(12), 15–20 (2005).
[21]P. Novák, J. C. Panitz, F. Joho, M. Lanz, R. Imhof, and M. Coluccia, "Advanced *in situ* methods for the characterization of practical electrodes in lithium-ion batteries," J. Power Sources **90**(1), 52–58 (2000).
[22]J.-C. Panitz, F. Joho, and P. Novák, "*In situ* characterization of a graphite electrode in a secondary lithium-ion battery using Raman microscopy," Appl. Spectrosc. **53**(10), 1188–1199 (1999).
[23]E. Plichta, S. Slane, M. Uchiyama, M. Salomon, D. Chua, W. B. Ebner, and H. W. Lin, "An improved Li/Li_xCoO_2 rechargeable cell," J. Electrochem. Soc. **136**(7), 1865–1869 (1989).
[24]J. N. Reimers and J. R. Dahn, "Electrochemical and *in situ* X-ray diffraction studies of lithium intercalation in Li_xCoO_2," J. Electrochem. Soc. **139**(8), 2091–2097 (1992).
[25]S. R. Sails, D. J. Gardiner, M. Bowden, J. Savage, and D. Rodway, "Monitoring the quality of diamond films using Raman spectra excited at 514.5 nm and 633 nm," Diamond Relat. Mater. **5**(68), 589–591 (1996).
[26]Q. Shi, Y. Takahashi, J. Akimoto, I. C. Stefan, and D. A. Scherson, "*In situ* Raman scattering measurements of a $LiMn_2O_4$ single crystal microelectrode," Electrochem. Solid-State Lett. **8**(10), A521–A524 (2005).